

The Hubble Deep Field and the Early Evolution of Galaxies

Piero Madau

Space Telescope Science Institute, 3700 San Martin Drive, Baltimore, MD 21218

Abstract.

I review some recent progress made in our understanding of galaxy evolution and the cosmic history of star formation. The *Hubble Deep Field* (HDF) imaging survey has achieved the sensitivity to capture the bulk of the extragalactic background light from discrete sources. No evidence is found in the optical number-magnitude relation down to $AB = 29$ mag for a large amount of star formation at high redshifts. A census of the ultraviolet and blue “dropouts”, which requires the inclusion of the effects of intergalactic attenuation on the colors of cosmologically distant galaxies, appears to confirm this basic conclusion. The emission history of the universe at ultraviolet, optical, and near-infrared wavelengths can be modeled from the present epoch to $z \approx 4$ by tracing the evolution with cosmic time of the galaxy luminosity density, as determined from several deep spectroscopic samples and the HDF. The global spectrophotometric properties of field galaxies are well fitted by a simple stellar evolution model, defined by a time-dependent star formation rate (SFR) per unit comoving volume and a universal initial mass function which is relatively rich in massive stars. The SFR density is found to rise sharply, by about an order of magnitude, from a redshift of zero to a peak value at $z \approx 1.5$ in the range $0.12\text{--}0.17 \text{ M}_{\odot} \text{ yr}^{-1} \text{ Mpc}^{-3}$, to fall again by a factor of 2 (4) out of a redshift of 3 (4). Since only 10% of the current stellar content of galaxies is produced at $z > 2.5$, a rather low cosmic metallicity is predicted at these early times, in good agreement with the observed enrichment history of the damped Lyman- α systems. The biggest uncertainty is represented by the poorly constrained amount of starlight that was absorbed by dust and reradiated in the IR at early epochs. A “monolithic collapse” scenario, where half of the present-day stars formed at $z > 2.5$ and were shrouded by dust, can be made consistent with the global history of light, but appears to overpredict the metal mass density at high redshifts.

1. Introduction

Much observing time has been devoted in the past few years to the problem of the detection of galaxies at high redshifts, as it was anticipated that any knowledge of their early luminosity and color evolution would set important constraints on the history of structure and star formation in the universe. While it has become now

clear that blank-sky surveys for strong Ly α -emitting primeval galaxies are not particularly efficient (Djorgovski & Thompson 1993), the method of obtaining multicolor broadband observations of the emitter’s rest-frame UV and optical stellar continuum has been successfully applied to select galaxies at cosmological distances in ground-based surveys (Steidel & Hamilton 1992; Steidel et al. 1996a; see review by Pettini in this proceedings) and in the *Hubble Deep Field* (HDF) (Madau et al. 1996, hereafter M96; Steidel et al. 1996b; Lowenthal et al. 1997). Together with the tremendous progress in our understanding of faint galaxy data at $z \lesssim 1$ made possible by the recent completion of several comprehensive ground-based spectroscopic surveys (Lilly et al. 1995; Ellis et al. 1996; Cowie et al. 1996), the identification of star-forming galaxies at $2 \lesssim z \lesssim 4$ has provided new clues to some key questions of galaxy formation and evolution studies: Is there a characteristic epoch of star and metal formation in galaxies? What fraction of the luminous baryons observed today were already locked into galaxies at early epochs? Are high- z galaxies obscured by dust? Do spheroids form early and rapidly? Is there a “global” IMF? Through the systematic study of galaxies at increasing cosmological lookback times it has become possible to reconstruct the history of stellar birthrate *directly*, as opposite to the “classical” method where one studies the resolved stellar populations of the Milky Way and nearby galaxies and infers their evolutionary history from fossil records – well-known examples of this more traditional approach are nuclear cosmochronology, the color-magnitude diagram of globular clusters, the cooling sequence of white dwarfs (see Renzini 1993 and references therein).

In this talk I will review the broad picture that has recently emerged from the “direct” method, focusing on the emission properties at ultraviolet, optical, and near-IR wavelengths of the galaxy population *as a whole*. I will show how the combination of HST deep imaging and ground-based spectroscopy offers now an exciting first glimpse to the history of the conversion of neutral gas into stars in field galaxies. In the following, all magnitudes will be given in the AB system, and a flat cosmology with $q_0 = 0.5$ and $H_0 = 50 \text{ km s}^{-1} \text{ Mpc}^{-1}$ will be adopted.

2. The Hubble Deep Field

As the best view to date of the optical sky at faint flux levels, the HDF imaging survey has rapidly become a key testing ground for models of galaxy evolution. The field, an undistinguished portion of the northern sky at high galactic latitudes, was imaged for approximately 150 orbits from 18 to 30 December 1995 with the Wide Field Planetary Camera onboard the *Hubble Space Telescope*. With its depth – reaching 5- σ limiting AB magnitudes of roughly 27.7, 28.6, 29.0, and 28.4 in U, B, V , and I ¹ (Williams et al. 1996) – and four-filter strategy in order to detect Lyman-break galaxies at various redshifts, the HDF offers the opportunity to study the galaxy population in unprecedented detail.

¹This is roughly three magnitudes fainter than the deepest ground based images in the red bands, two magnitudes deeper in the blue, and one magnitude deeper in the ultraviolet.

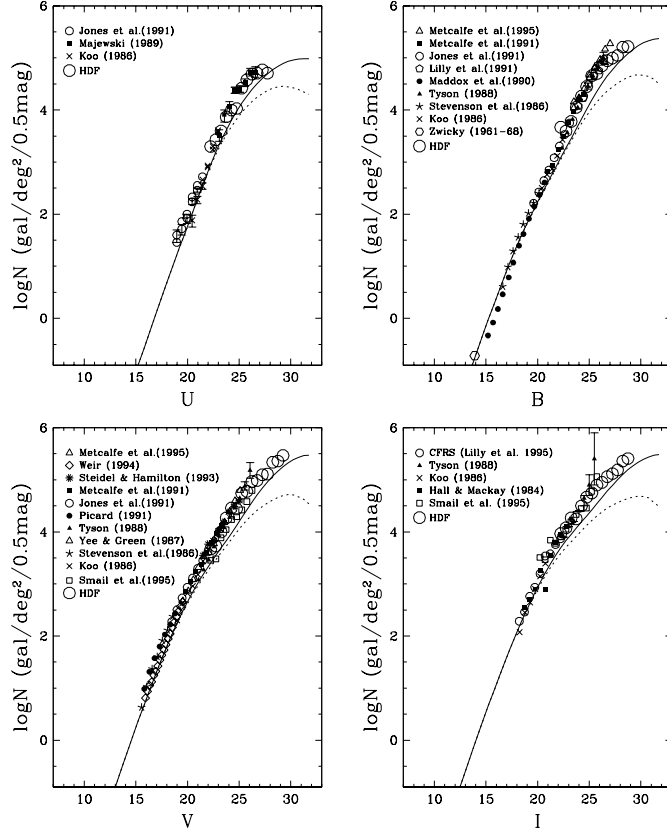


Figure 1. Differential galaxy number counts per square degree per half magnitude interval as a function of AB apparent magnitude. The sources of the data points are indicated in each panel (see Pozzetti et al. 1997 for the complete reference list). Note the decrease of the logarithmic slope $d \log N / dm$ at faint magnitudes. The curves show the well known deficiency of faint galaxies which characterizes no-evolution models in a $\Omega = 0$ (*solid line*) and $\Omega = 1$ (*dotted line*) universe.

2.1. Galaxy Counts and the EBL

There are about 3,000 galaxies in the HDF, corresponding to $2 \times 10^6 \text{ deg}^{-2}$ to $V \approx 29$ mag. The galaxy counts as a function of AB isophotal magnitude are shown in Figure 1 in the F300W, F450W, F606W, and F814W bandpasses (the number corresponds to the central wavelength in nm) for all galaxies with signal-to-noise ratio $S/N > 3$ within the band (Williams et al. 1996). A compilation of existing ground-based data is also shown, together with the predictions of no-evolution models, i.e. models in which the absolute brightness, volume density, and spectra of galaxies do not change with time. The HDF counts are plotted down to the 80% completeness limit and are found to agree reasonably well with previous surveys, to within 20% in the magnitude range $22 < AB < 26$. In all four bands, the slope α of the differential galaxy counts, $\log N(m) = \alpha m$, flattens at faint magnitudes, e.g., from $\alpha = 0.45$ in the interval $21 < B < 25$ to $\alpha = 0.17$ for $25 < B < 29$. This feature cannot be due to the reddening of distant sources as their Lyman break gets redshifted into the blue passband, since the fraction of Lyman-break galaxies at $B \sim 25$ is only of order 10% (cf. Guhathakurta et al. 1990). Moreover, an absorption-induced loss of sources could not explain the similar flattening of the number-magnitude relation observed in the V and I bands. Rather, the change of slope suggests a decline in the surface density of luminous galaxies beyond $z \sim 1.5$.

The contribution of known galaxies to the extragalactic background light (EBL) – an indicator of the total optical luminosity of the universe – can be calculated directly by integrating the emitted flux times the differential galaxy number counts down to the detection threshold. The leveling off of the counts is clearly seen in Figure 2, where the function $i_\nu = 10^{-0.4(m+48.6)} \times N(m)$ is plotted against apparent magnitude in all bands (Pozzetti et al. 1997). While counts having a logarithmic slope of $\alpha \geq 0.40$ continue to add to the EBL at the faintest magnitudes, it appears that the HDF survey has achieved the sensitivity to capture the bulk of the extragalactic light from discrete sources (an extrapolation of the observed counts to brighter and/or fainter magnitudes would typically increase the sky brightness by less than 20%). To $AB = 29$, the sky brightness from resolved galaxies in the I -band is $\approx 2 \times 10^{-20} \text{ ergs cm}^{-2} \text{ s}^{-1} \text{ Hz}^{-1} \text{ sr}^{-1}$, increasing roughly as λ^2 from 2000 to 8000 Å. The flattening of the number counts has the interesting consequences that the galaxies that produce $\sim 60\%$ of the blue EBL have $B < 24.5$. They are then bright enough to be identified in spectroscopic surveys, and are indeed known to have median redshift $\langle z \rangle = 0.6$ (Lilly et al. 1995). The quite general conclusion is that there is no evidence in the number-magnitude relation down to very faint flux levels for a large amount of star formation at high redshift. Note that these considerations do not constrain the *rate* of starbirth at early epochs, only the total (integrated over cosmic time) amount of stars – hence background light – being produced, and *neglect the effect of dust reddening*.

2.2. Intergalactic Absorption

A more direct way to track galaxy evolution at early epochs is through a census of the HDF “dropouts”. At faint magnitudes, the interpretation and detailed modeling of the observations require the self-consistent inclusion of the effect of intergalactic attenuation on galaxy colors. Absorption by intervening material

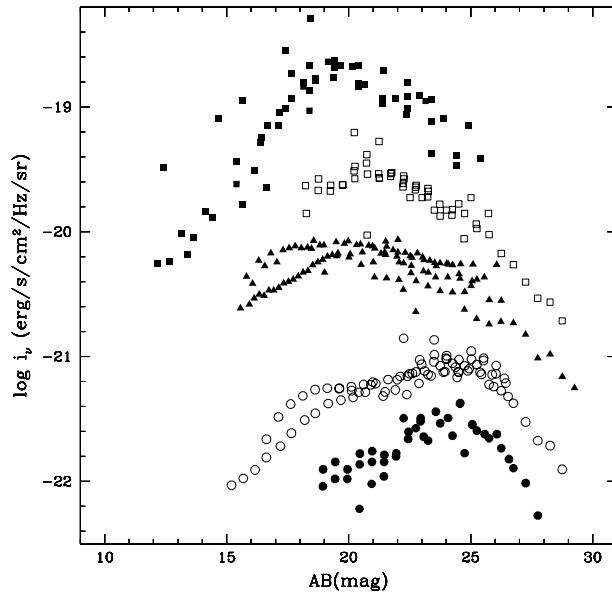


Figure 2. The contribution of known galaxies to the extragalactic background light per magnitude bin as a function of U (*filled circles*), B (*open circles*), V (*filled triangles*), I (*open squares*) and K (*filled squares*) magnitudes. For clarity, the B , V , I and K values have been multiplied by a factor of 2, 8, 20, and 40, respectively.

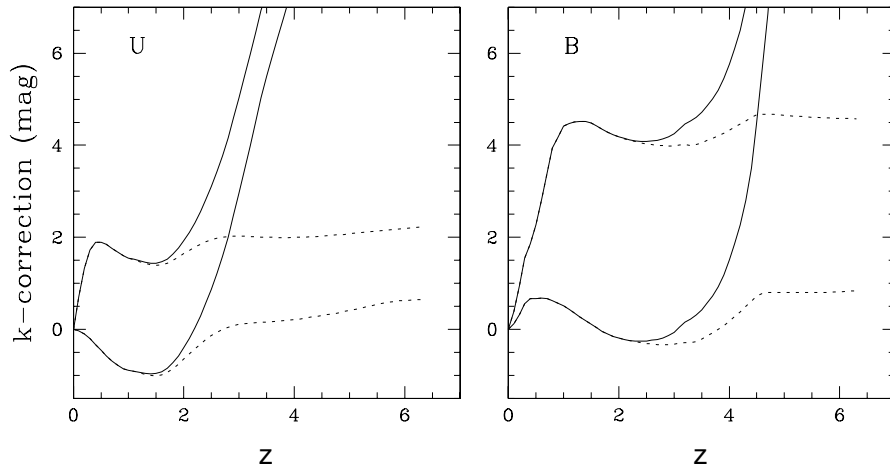


Figure 3. Average k -correction in the U and B bands for elliptical and late-type spiral galaxies as a function of redshift. *Dotted lines*: unattenuated synthetic spectra. *Solid lines*: spectra modified by intergalactic absorption.

has been known for quite some time to distort our view of objects at cosmological distances. It has been realized only recently, however, that the accumulated line-blanketing and Lyman-continuum absorption from the Ly α forest clouds and Lyman-limit systems along the path to high redshifts can be efficiently used to identify galaxies at $z \gtrsim 2$ (Madau 1995; Steidel & Hamilton 1992). Although other spectral features, such as the 4000 Å and 912 Å breaks which characterize the integrated spectra of stellar populations, with the latter possibly enhanced by self-absorption from interstellar gas within the galaxy itself, can and have been used as tracers of redshifts, the model predictions of their magnitude are sensitive to the unknown physical and evolutionary state of the galaxy, i.e., its star formation history, age, and H I distribution, and hence are subject to substantial uncertainties. By contrast, the “reddening” effect due to atomic processes in cosmological distributed QSO absorption systems is ubiquitous and can be reliably taken into account. While stochastic in nature, r.m.s. fluctuations away from the mean opacity are bound to be modest in most situations, due to the broadband nature of the adopted filter set.

The magnitude and cosmological importance of intergalactic absorption on galaxy spectra can be effectively illustrated by including its effect in the standard k -correction term needed to translate the galaxy magnitude at Earth into its

rest-frame value,

$$k(z) = -2.5 \log \left[(1+z) \frac{L(\nu)}{L(\nu_{\text{obs}})} \langle e^{-\tau} \rangle \right], \quad (1)$$

where $L(\nu)$ is the specific power emitted by a source at redshift z , $\nu_{\text{obs}} = \nu/(1+z)$, $\langle e^{-\tau} \rangle$ is the cosmic transmission averaged over all lines of sight, and we have assumed no intrinsic luminosity evolution. Figure 3 shows the k -correction in the U and B HDF bands as a function of redshift for synthetic spectra of galaxies which well reproduce the colors of present-day ellipticals and spirals. The effect at high redshift is huge. Due to intergalactic attenuation alone, the k -correction in the F300W bandpass increases by as much as 4 magnitudes between $z \approx 2$ and $z \approx 3.5$, giving origin to a “UV dropout”. In the F450W band, the increase is barely noticeable at $z \approx 3$, but becomes very large above $z \approx 4$, thereby producing a “blue dropout”.

2.3. Ultraviolet and Blue Dropouts

Ground-based observations have used color techniques which are sensitive to the presence of a Lyman-continuum break superposed to an otherwise flat UV spectrum to identify galaxies at $z \approx 3$ (Steidel & Hamilton 1992; Steidel et al. 1996a). New photometric criteria for robustly selecting Lyman-break galaxies have been developed based on the HDF color system, providing what appear to be largely uncontaminated samples of star-forming galaxies at high redshifts (M96). The HDF ultraviolet passband – which is bluer than the standard ground-based U filter – permits the identification of star-forming galaxies in the interval $2 < z < 3.5$ (Figure 4). Galaxies in this redshift range predominantly occupy the top left portion of the $U - B$ vs. $B - I$ color-color diagram because of the attenuation by the intergalactic medium and intrinsic extinction. Galaxies at lower redshift can have similar $U - B$ colors, but they are typically either old or dusty, and are therefore red in $B - I$ as well. Of order 100 (200) ultraviolet dropouts can be identified in the HDF which are brighter than $B = 27$ ($B = 29$), approximately 25% (20%) of the total. To date, about 25 among the brightest ones have spectroscopically confirmed redshift in the range $2.0 < z < 3.4$. The color-selection region is illustrated in Figure 5. The UBI criteria isolate objects that have relatively blue colors in the optical, but a sharp drop into the UV. In analogous way, the blue passband allows the selection of candidate star-forming galaxies in the interval $3.5 < z < 4.5$. Only ~ 20 (60) B dropouts down to $V = 28$ ($V = 30$) have been identified in the $B - V$ vs. $V - I$ plane (M96). The brightest one has recently been confirmed through deep Keck spectroscopy to be at $z = 4.02$ (Dickinson 1997), consistent with the photometric predictions.

The UV continuum emission from a galaxy with significant ongoing star formation is entirely dominated by late-O/early-B stars on the main sequence, which have masses $\gtrsim 10 M_{\odot}$ and lifetimes $t_{MS} \lesssim 2 \times 10^7$ yr. After an initial transient phase where the UV flux rises rapidly and the turnoff mass drops below $10 M_{\odot}$, a steady state is reached where the measured luminosity becomes proportional to the instantaneous SFR and independent of the past star formation history (see Madau, Pozzetti, & Dickinson 1997). Figure 6 depicts the present-epoch “SFR function” – which describes the number of star-forming galaxies as a function of their ongoing SFR –, together with the derived distribution of

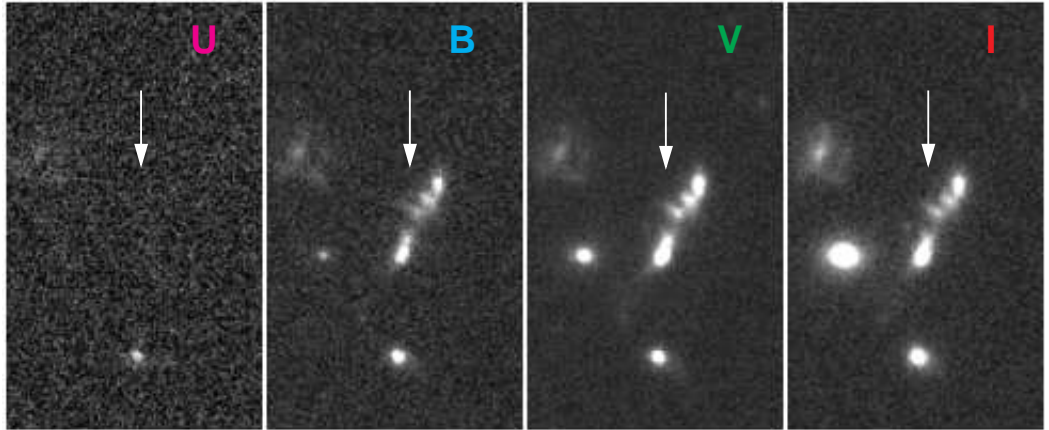
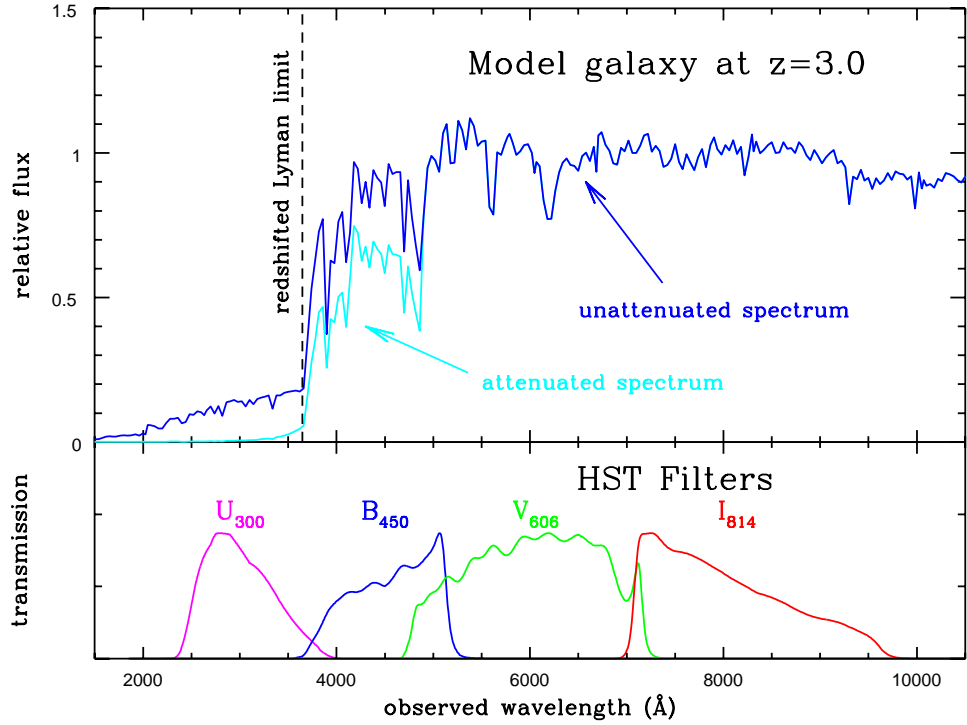


Figure 4. Synthetic spectrum of a star-forming galaxy at $z = 3$, superimposed on the throughput curves of the HDF filters. Such a galaxy would appear blue in its optical colors but would be virtually undetected in the ultraviolet filter. At higher redshifts ($z \gtrsim 4$), a similar galaxy would vanish from the blue filter. *Bottom panel:* $U, B, V,$ and I images of an identified UV dropout at $z = 2.8$. (Courtesy of M. Dickinson.)

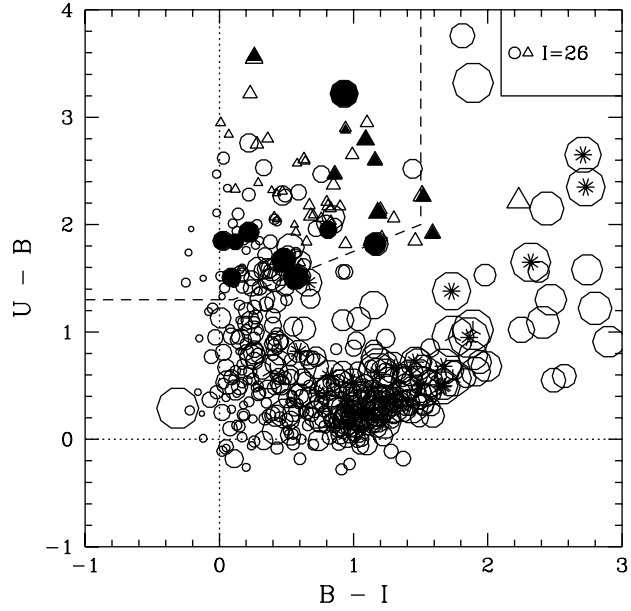


Figure 5. Color-color plot of galaxies in the HDF with $B < 27$. Objects undetected in U (with $S/N < 1$) are plotted as triangles at the 1σ lower limits to their $U - B$ colors. Symbols size scales with the I mag of the object. The dashed lines outline the selection region within which we identify candidate $2 < z < 3.5$ objects. Galaxies with spectroscopically confirmed redshifts within this range (Steidel et al. 1996b; Lowenthal et al. 1997) are marked as solid symbols. Galaxies having confirmed redshifts less than 2 (Cohen et al. 1996) are marked as asterisks. Note that no low-redshift interlopers have been found among the high-redshift sample.

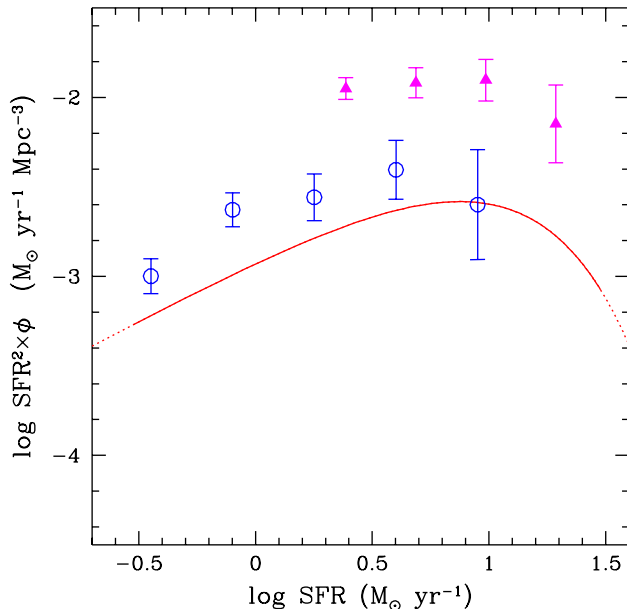


Figure 6. Distribution of star formation rates at different redshifts. *Filled triangles*: HDF ultraviolet dropouts at $\langle z \rangle = 2.75$. *Empty circles*: HDF blue dropouts at $\langle z \rangle = 4$. The curve represents the best-fit Schechter function from the Gallego et al. (1995) $H\alpha$ survey at $z = 0$.

stellar birthrates for the HDF ultraviolet and blue dropouts. The comparison shows the sign of a significant density evolution – a rapid increase in ϕ_* .

3. Evolution of the Galaxy Luminosity Density

The integrated light radiated per unit volume from the entire galaxy population is an average over cosmic time of the stochastic, possibly short-lived star formation episodes of individual galaxies, and should follow a relatively simple dependence on redshift. In the UV – where it is proportional to the global star formation rate (SFR) – its evolution should provide information, e.g., on the mechanisms which may prevent the gas within virialized dark matter halos to radiatively cool and turn into stars at early times, or on the epoch when galaxies exhausted their reservoirs of cold gas. From a comparison between different wavebands it should be possible to set constraints on the average initial mass function (IMF) and dust content of galaxies.

The comoving luminosity density, $\rho_\nu(z)$, from the present epoch to $z \approx 4$ is shown in Figure 7 in five broad passbands centered around 0.15, 0.28, 0.44, 1.0, and 2.2 μm . The data are taken from the K -selected wide-field redshift survey of Gardner et al. (1997), the I -selected CFRS (Lilly et al. 1996) and B -selected Autofib (Ellis et al. 1996) surveys, the photometric redshift catalog for the HDF

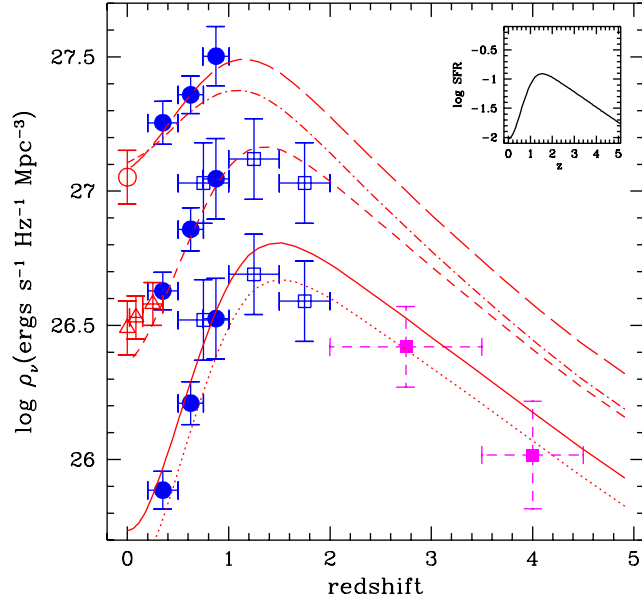


Figure 7. Evolution of the luminosity density at rest-frame wavelengths of 0.15 (*dotted line*), 0.28 (*solid line*), 0.44 (*short-dashed line*), 1.0 (*long-dashed line*), and 2.2 (*dot-dashed line*) μm . The data points with error bars are taken from Lilly et al. (1996) (*filled dots*), Connolly et al. (1997) (*empty squares*), M96 and Madau (1997) (*filled squares*), Ellis et al. (1996) (*empty triangles*), and Gardner et al. (1997) (*empty dot*). The inset in the upper-right corner of the plot shows the SFR density ($\text{M}_{\odot} \text{yr}^{-1} \text{Mpc}^{-3}$) versus redshift which was used as input to the population synthesis code. The model assumes a Salpeter IMF, SMC-type dust in a foreground screen, and a universal $E(B - V) = 0.06$.

of Connolly et al. (1997) – which take advantage of deep infrared observations by Dickinson et al. (1997) – and the color-selected UV and blue “dropouts” of M96 (see also Madau 1997). They have all been corrected for incompleteness by integrating over the best-fit Schechter function in each redshift bin,

$$\rho_\nu(z) = \int_0^\infty L\phi(L, z)dL = \Gamma(2 + \alpha)\phi_*L_*. \quad (2)$$

As from the Connolly et al. (1997) and M96 data sets it is not possible to reliably determine the faint end slope of the luminosity function, a value of $\alpha = -1.3$ has been assumed at each redshift interval for comparison with the CFRS sample (Lilly et al. 1995). The error bars are typically less than 0.2 in the log, and reflect the uncertainties present in these corrections and, in the HDF $z > 2$ sample, in the volume normalization and color-selection region. In the K -band, the determination by Gardner et al. (1997) agrees to within 30% with Cowie et al. (1996), and we have assigned an error of 0.1 in the log to the estimate of the local luminosity density at $2.2 \mu\text{m}$. Despite the obvious caveats due to the likely incompleteness in the data sets, different selection criteria, and existence of systematic uncertainties in the photometric redshift technique, the spectroscopic, photometric, and Lyman-break galaxy samples appear to provide a remarkably consistent picture of the emission history of field galaxies. The UV luminosity density rises sharply, by about an order of magnitude, from a redshift of zero to a peak at $z \approx 1.5$, to fall again by a factor of 2 (4) out to a redshift of 3 (4) (M96; Lilly et al. 1996; Connolly et al. 1997). This points to a rapid drop in the volume-averaged SFR in the last 8–10 Gyr, and to a redshift range $1 \lesssim z \lesssim 2$ in which the bulk of the stellar population was assembled. The decline in brightness at late epochs is shallower at longer wavelengths, as galaxies becomes redder with cosmic time, on the average.

4. Stellar Population Synthesis Modeling

Stellar population synthesis has become a standard technique to study the spectrophotometric properties of galaxies. In the following, I will make extensive use of the latest version of Bruzual & Charlot (1993) isochrone synthesis code, optimized with an updated library of stellar spectra (Bruzual & Charlot 1997), to predict the time change of the spectral energy distribution of a stellar population. The uncertainties linked to the underlying stellar evolution prescriptions and the lack of accurate flux libraries do not typically exceed 35% (Charlot, Worthey, & Bressan 1966). I will consider three possibilities for the IMF, $\phi(m) \propto m^{-1-x}$: a Salpeter (1955) function ($x = 1.35$), a Scalo (1986) function, which is flatter for low-mass stars and significantly less rich in massive stars than Salpeter, and an intermediate case with $x = 1.7$. In all models the metallicity is fixed to *solar* values and the IMF is truncated at 0.1 and $125 M_\odot$.

An interesting question now arises as to whether a simple stellar evolution model, defined by a time-dependent SFR per unit volume and a constant IMF, may reproduce the global UV, optical, and near-IR photometric properties of the universe as given in Figure 7. In a stellar system with arbitrary star formation

rate, the luminosity density at time t is given by the convolution integral

$$\rho_\nu(t) = \int_0^t L_\nu(\tau) \times \text{SFR}(t - \tau) d\tau, \quad (3)$$

where $L_\nu(\tau)$ is the specific luminosity radiated per unit initial mass by a generation of stars with age τ . In the instantaneous recycling approximation (Tinsley 1980), the total stellar mass density produced at time t is

$$\rho_s(t) = (1 - R) \int_0^t \text{SFR}(t) dt, \quad (4)$$

where R is the mass fraction of a generation of stars that is returned to the interstellar medium, $R \approx 0.3, 0.15$, and 0.2 for a Salpeter, $x = 1.7$, and Scalo IMF, respectively.

In computing the time evolution of the spectrophotometric properties of a stellar population in comoving volumes large enough to be representative of the universe as a whole, our first task is to relate the observed UV emission to a mean star formation rate. This is done by assuming a universal IMF and then fitting a smooth function to the UV continuum emissivity at various redshifts. By construction, all models will therefore produce, to within the errors, the right amount of ultraviolet light. Bruzual and Charlot’s synthesis code can then be used to predict the cosmic emission history at long wavelengths. It is fair to point out some of the limitations of this approach at the outset. (1) It focuses on the emission properties of “normal”, optically-selected field galaxies which are only moderately affected by dust – a typical spiral emits 30% of its energy in the far-infrared region (Soifer & Neugebauer 1991) –. Starlight which is completely blocked from view even in the near-IR by a large optical depth in dust is not recorded by this technique, and the associated baryonic mass and metals missed from our census. The contribution of infrared-selected dusty starbursts to the integrated stellar mass density cannot be large, however, for otherwise the current limits to the energy density of the mid- and far-infrared background would be violated (Puget et al. 1996; Kashlinsky, Mather, & Odenwald 1996; Fall, Charlot, & Pei 1996; Guiderdoni et al. 1997). Locally, infrared luminous galaxies are known to produce only a small fraction of the IR luminosity of the universe (Soifer & Neugebauer 1991). (2) While the method bypasses the ambiguities associated with the study of morphologically-distinct samples whose physical significance remains unclear, by the same token it does not provide any *direct* information on the processes which shaped the Hubble sequence. (3) Although in all our calculations the IMF extends from 0.1 to $125 M_\odot$, by modeling the rest-frame galaxy luminosity density from 0.15 to $2.2 \mu\text{m}$ we are actually only sensitive to stars within the mass range from ~ 0.8 to about $20 M_\odot$. This introduces non-negligible uncertainties in our estimates of the total amount of stars and metals produced. (4) No attempt has been made to include the effects of cosmic chemical evolution on the predicted galaxy colors. All the population synthesis models assume solar metallicity and will therefore generate colors at early epochs that are too red. (5) The uncertainties present in the estimates of the UV luminosity density from the identification of Lyman-break galaxies in the HDF are quite large, and the data points at $z > 2$ should still be regarded as tentative. This is especially true for the faint blue dropout sample at

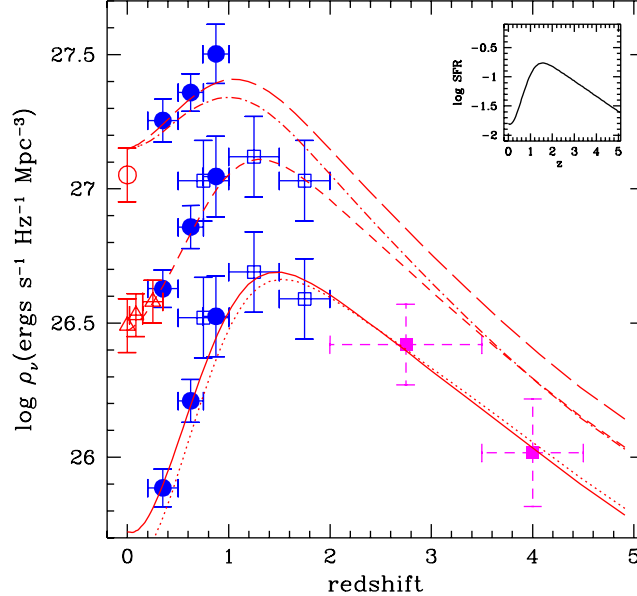


Figure 8. Same as in Figure 6, but assuming an IMF with $\phi(m) \propto m^{-1-1.7}$ and no dust extinction.

$\langle z \rangle = 4$, where only one spectroscopic confirmation has been obtained so far. On the other hand, there is no evidence for a gross mismatch at the $z \approx 2$ transition between the photometric redshift sample of Connolly et al. (1997) and the M96 ultraviolet dropout sample.

4.1. Salpeter IMF

Figure 7 shows the model predictions for the evolution of ρ_ν at rest-frame ultraviolet to near-infrared frequencies. In the absence of dust reddening, this relatively flat IMF generates spectra that are too blue to reproduce the observed mean galaxy colors. The shape of the predicted and observed $\rho_\nu(z)$ relations agrees better to within the uncertainties if some amount of dust extinction, $E(B-V) = 0.06$, is included. In this case, the observed UV luminosities must be corrected upwards by a factor of 1.4 at 2800 Å and 2.1 at 1500 Å. As expected, while the ultraviolet emissivity traces remarkably well the rise, peak, and sharp drop in the instantaneous star formation rate (the smooth function shown in the inset on the upper-right corner of the figure), an increasingly large component of the longer wavelengths light reflects the past star formation history. The peak in the luminosity density at 1.0 and 2.2 μm occurs then at later epochs, while the decline from $z \approx 1$ to $z = 0$ is more gentle than observed at shorter wavelengths. The total stellar mass density at $z = 0$ is $\rho_s(0) = 3.7 \times 10^8 M_\odot \text{Mpc}^{-3}$, with a fraction close to 65% being produced at $z > 1$, and only 20% at $z > 2$. In the

assumed cosmology, about half of the stars observed today are more than 9 Gyr old, and only 20% are younger than 5 Gyr.²

4.2. $x=1.7$ IMF

Figure 8 shows the model predictions for a $x = 1.7$ IMF and negligible dust extinction. While able to reproduce quite well the B -band emission history and consistent within the error with the local K -band light, this model slightly underestimates the $1 \mu\text{m}$ luminosity density at $z \approx 1$. The total stellar mass density today is larger than in the previous case, $\rho_s(0) = 6.2 \times 10^8 \text{ M}_\odot \text{ Mpc}^{-3}$.

4.3. Scalo IMF

The fit to the data is found to be much poorer for a Scalo function, since this IMF generates spectra that are too red to reproduce the observed mean galaxy colors, as already noted by Lilly et al. (1996). Because of the relatively large number of solar mass stars formed, it produces too much long-wavelength light by the present epoch (Madau et al. 1997). The addition of dust reddening would obviously make the fit even worse.

4.4. The Brightness of the Night Sky

Our modeling of the data points to a redshift range $1 \lesssim z \lesssim 2$ where the bulk of the stellar mass was actually produced. The uncertainties in the determination of the luminosity density at that epoch are, however, quite large. At $z \approx 1$, the increase in the “estimated” emissivity (i.e., corrected for incompleteness by integrating over the best-fit Schechter function) over that “directly” observed in the CFRS galaxy sample is about a factor of 2 (Lilly et al. 1996). Between $z = 1$ and $z = 2$, the peak in the average SFR is only constrained by the photometric redshifts of Connolly et al. (1997) and by the HDF UV dropout sample, both of which may be subject to systematic biases.

An important check on the inferred emission history of field galaxies comes from a comparison of the EBL produced by known galaxies (see §2.1) and the predicted mean surface brightness of the night sky,

$$I_\nu = \frac{1}{4\pi} \int_0^\infty dz \frac{dl}{dz} \rho_{\nu'}(z) \quad (5)$$

where $\nu' = \nu(1+z)$ and dl/dz is the cosmological line element. The results are plotted in Figure 9. The overall agreement is remarkably good, with the model spectra being only slightly bluer, by about 20–30%, than the observed EBL. The straightforward conclusion of this exercise is that the star formation histories depicted in Figures 7 and 8 appear able to account for the entire background light recorded in the galaxy counts down to the very faint magnitudes probed by the HDF.

²Note that, contrary to the measured number densities of objects and rates of star formation, the integrated stellar mass density does not depend on the assumed cosmological model.

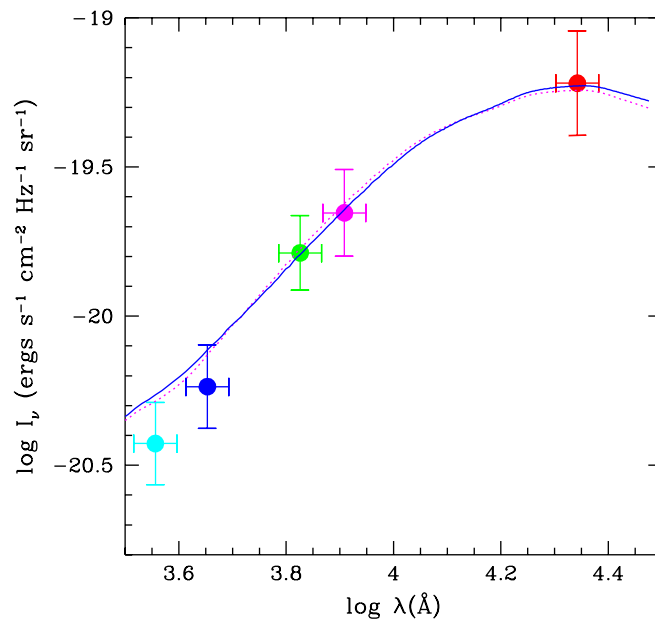


Figure 9. Spectrum of the extragalactic background light as derived from a compilation of ground-based and HDF galaxy counts (see Pozzetti et al. 1997). The 2σ error bars arise mostly from field-to-field variations. *Solid line*: Model predictions for a Salpeter IMF and $E(B - V) = 0.06$ (star formation history of Figure 7). *Dotted line*: Model predictions for a $x = 1.7$ IMF and negligible dust extinction (star formation history of Figure 8).

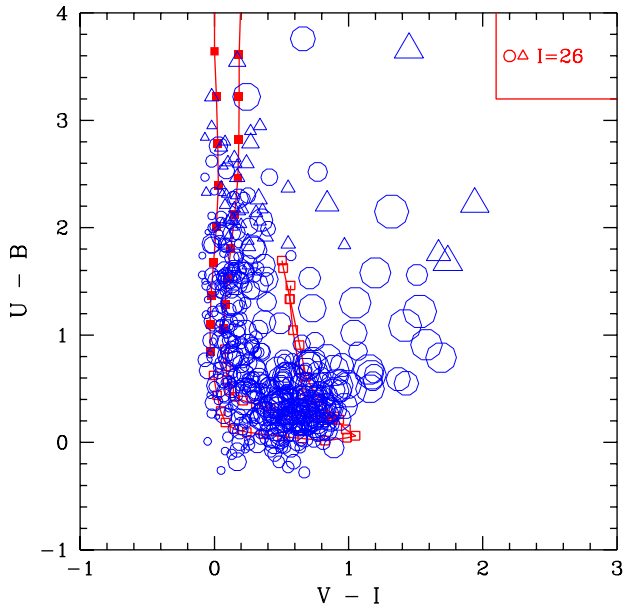


Figure 10. *Solid lines*: model predictions for the color evolution of galaxies according to the star formation histories of Figure 7 (*right curve*) and 8 (*left curve*). The points (*filled squares* for $z > 2$ and *empty squares* for $z < 2$) are plotted at redshift interval $\Delta z = 0.1$. *Empty circles* and *triangles*: colors of galaxies in the HDF with $22 < B < 27$. The symbol types and sizes are as described for Figure 5. The “plume” of reddened high- z galaxies is clearly seen in the data.

4.5. The Colors of High-Redshift Galaxies

Figure 10 shows a comparison between the HDF data and the model predictions for the evolution of galaxies in the $U - B$ vs. $V - I$ color-color plane according to the star formation histories of Figures 7 and 8. The fact that the Salpeter IMF, $E(B - V) = 0.06$ model reproduces quite well the rest-frame UV colors of high- z galaxies, while a dust-free $x = 1.7$ IMF generates $V - I$ colors that are 0.2 mag too blue, suggests the presence of some amount of dust extinction in Lyman-break galaxies at $z \sim 3$ (cf. Meurer et al. 1997).

4.6. The Stellar Mass Density Today

The best-fit models discussed in § 4 generate a present-day stellar mass density in the range between 4 and $6 \times 10^8 M_{\odot} \text{Mpc}^{-3}$. Although one could in principle lower this number by adopting a top-heavy IMF, richer in massive UV-producing stars, in practice a significant amount of dust reddening – hence of “hidden” star formation – would then be required to match the observed galaxy colors. The net effect of this operation would be a baryonic mass comparable to the estimate above and a far too large infrared background (see below). It appears therefore

that the observed galaxy emission history implies a stellar mass density at the present epoch in the interval $0.005 \lesssim \Omega_s h_{50}^2 \lesssim 0.009$. The stellar mass-to-light ratios range from 4.5 in the B -band and 0.9 in K for a Salpeter function, to 8.1 in B and 1.5 in K for a $x = 1.7$ IMF. Note that these values are quite sensitive to the lower-mass cutoff of the IMF, as very-low mass stars can contribute significantly to the mass but not to the integrated light of the whole stellar population. A lower cutoff of $0.2 M_\odot$, instead of the $0.1 M_\odot$ adopted, would decrease the mass-to-light ratio by a factor of 1.3 for a Salpeter function, 1.6 for $x = 1.7$, and 1.1 for a Scalo IMF.

5. Star Formation at High Redshift: Monolithic Collapse Versus Hierarchical Clustering Models

The significant uncertainties present in the estimates of the star formation density at $z > 2$ have already been mentioned. The biggest one is probably associated with dust reddening, but, as the color-selected HDF sample includes only the most actively star-forming young objects, one could also imagine the existence of a large population of relatively old or faint galaxies still undetected at high- z . The issue of the amount of star formation at early epochs is a non trivial one, as the two competing models, “monolithic collapse” versus hierarchical clustering, make very different predictions in this regard. From stellar population studies we know in fact that about half of the present-day stars are contained into spheroidal systems, i.e., elliptical galaxies and spiral galaxy bulges (Schechter & Dressler 1987). In the “monolithic” scenario these formed early and rapidly, experiencing a bright starburst phase at high- z (Eggen, Lynden-Bell, & Sandage 1962; Tinsley & Gunn 1976; Bower et al. 1992). In hierarchical clustering theory instead ellipticals form continuously by the merger of disk/bulge systems (Kauffman et al. 1993; White & Frenk 1991), and most galaxies never experience star formation rates in excess of a few solar masses per year (Baugh et al. 1997). The star formation histories discussed in § 4 produce only 10% of the current stellar content of galaxies at $z > 2.5$, in apparent agreement with hierarchical clustering cosmologies. In fact, the tendency to form the bulk of the stars at relatively low redshifts is a generic feature not only of the $\Omega_0 = 1$ CDM cosmology, but also of successful low-density CDM models (cf Figure 21 of Cole et al. 1994; Baugh et al. 1997).

It is then of interest to ask how much larger could the volume-averaged SFR at high- z be before its fossil records – in the form of long-lived, near solar-mass stars – became easily detectable as an excess of K -band light at late epochs. In particular, is it possible to envisage a toy model where 50% of the present-day stars formed at $z > 2.5$ and were shrouded by dust? The predicted emission history from such a model is depicted in Figure 11. To minimize the long-wavelength emissivity associated with the radiated ultraviolet light, a Salpeter IMF has been adopted. Consistency with the HDF data has been obtained assuming a dust extinction which increases rapidly with redshift, $E(B - V) = 0.0067(1 + z)^{2.2}$. This results in a correction to the rate of star formation of a factor ~ 5 at $z = 3$ and ~ 15 at $z = 4$. The total stellar mass density today is $\rho_s(0) = 5.0 \times 10^8 M_\odot \text{Mpc}^{-3}$ ($\Omega_s h_{50}^2 = 0.007$).

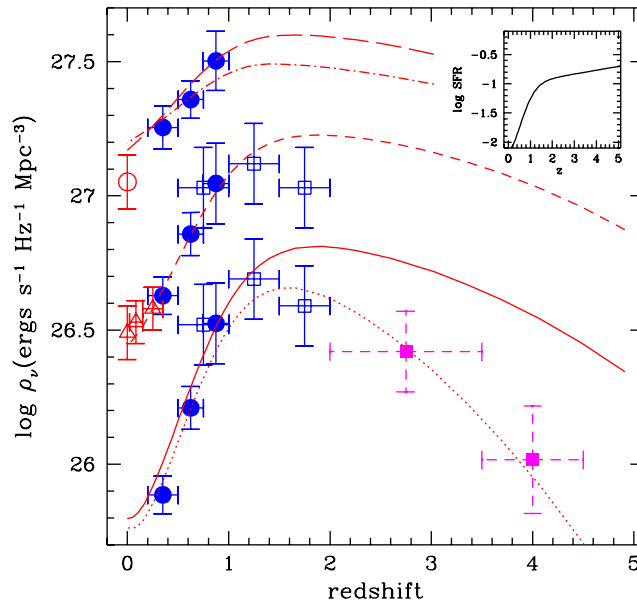


Figure 11. Test case with a much larger star formation density at high redshift than indicated by the HDF dropout analysis. The model – designed to mimick a “monolithic collapse” scenario – assumes a Salpeter IMF and a dust opacity which increases rapidly with redshift, $E(B - V) = 0.0067(1 + z)^{2.2}$. Notation is the same as in Figure 7.

Overall, the fit to the data is still acceptable, showing how the blue and near-IR light at $z < 1$ are relatively insensitive to significant variations in the SFR at high redshifts, and are then, because of the short timescale available at $z \gtrsim 2$, *relatively poor indicators of the star formation history at early epochs*. Note, however, that the adopted extinction-redshift relation implies negligible reddening at $z \lesssim 1$. Relaxing this – likely unphysical – assumption would cause the model to significantly overproduce the K -band local luminosity density. We have also checked that a larger amount of hidden star formation at early epochs would generate too much blue, $1 \mu\text{m}$ and $2.2 \mu\text{m}$ light to be still consistent with the observations. An IMF which is less rich in massive stars would only exacerbate the discrepancy.

5.1. Constraints from the Mid- and Far-Infrared Background

Ultimately, it should be possible to set some constraints on the total amount of star formation hidden by dust over the entire history of the universe by looking at the cosmic infrared background (CIB). From an analysis of the smoothness of the *COBE* DIRBE maps, Kashlinsky et al. (1996) have recently set an upper limit to the CIB of $10\text{--}15 \text{ nW m}^{-2} \text{ sr}^{-1}$ at $\lambda = 10\text{--}100 \mu\text{m}$ assuming clustered sources which evolve according to typical scenarios. An analysis using data from

COBE FIRAS by Puget et al. (1996) has produced a tentative detection at a level of $3.4 (\lambda/400\mu\text{m})^{-3} \text{ nW m}^{-2} \text{ sr}^{-1}$ in the 400–1000 μm range. By comparison, the integrated light that is reprocessed by dust in the model depicted in Figure 7 is close to $8 \text{ nW m}^{-2} \text{ sr}^{-1}$. The monolithic collapse scenario of Figure 11 generates about $6.5 \text{ nW m}^{-2} \text{ sr}^{-1}$ instead. While both these models appear to be consistent with the data (given the large uncertainties associated with the subtraction of foreground emission and the spectral shape of the CIB), it is clear that a significantly larger amount of hidden star formation at early and/or late epochs would overproduce the IR background (Fall et al. 1996; Guiderdoni et al. 1997).

5.2. Metal Production

We may at this stage use our set of models to establish a cosmic timetable for the production of heavy elements ($Z \geq 6$) in relatively bright field galaxies. What we are interested in here is the universal rate of ejection of newly synthesized material. In the approximation of instantaneous recycling, the metal ejection rate per unit comoving volume can be written as

$$\dot{\rho}_Z = y(1 - R) \times \text{SFR}, \quad (6)$$

where the *net*, IMF-averaged yield of returned metals is

$$y = \frac{\int m p_{\text{zm}} \phi(m) dm}{(1 - R) \int m \phi(m) dm}, \quad (7)$$

p_{zm} is the stellar yield, i.e., the mass fraction of a star of mass m that is converted to metals and ejected, and the dot denotes differentiation with respect to cosmic time.

The predicted end-products of stellar evolution, particularly from massive stars, are subject to significant uncertainties. These are mainly due to the effects of initial chemical composition, mass-loss history, the mechanisms of supernova explosions, and the critical mass, M_{BH} , above which stars collapse to black holes without ejecting heavy elements into space (Maeder 1992; Woosley & Weaver 1995). The IMF-averaged yield is also very sensitive to the choice of the IMF slope and lower-mass cutoff. Observationally, the best-fit “effective yield” (derived assuming a closed box model) is $0.025Z_{\odot}$ for Galactic halo clusters, $0.3Z_{\odot}$ for disk clusters, $0.4Z_{\odot}$ for the solar neighborhood, and $1.8Z_{\odot}$ for the Galactic bulge (Pagel 1987). The latter value may represent the universal true yield, while the lower effective yields found in the other cases may be due, e.g., to the loss of enriched material in galactic winds.

Figure 12 shows the total mass of metals ever ejected, ρ_Z , versus redshift, i.e., the sum of the heavy elements stored in stars and in the gas phase as given by the integral of equation (6) over cosmic time. The values plotted have been computed from the star formation histories depicted in Figures 7 and 11, and have been normalized to $y\rho_s(0)$, the mass density of metals at the present epoch according to each model. A characteristic feature of the two competing scenarios is the rather different average metallicity expected at high redshift. For comparison, we have also plotted the *gas metallicity*, Z_{DLA}/Z_{\odot} , as deduced from observations by Pettini et al. (1997) of the damped Lyman- α systems (DLAs).

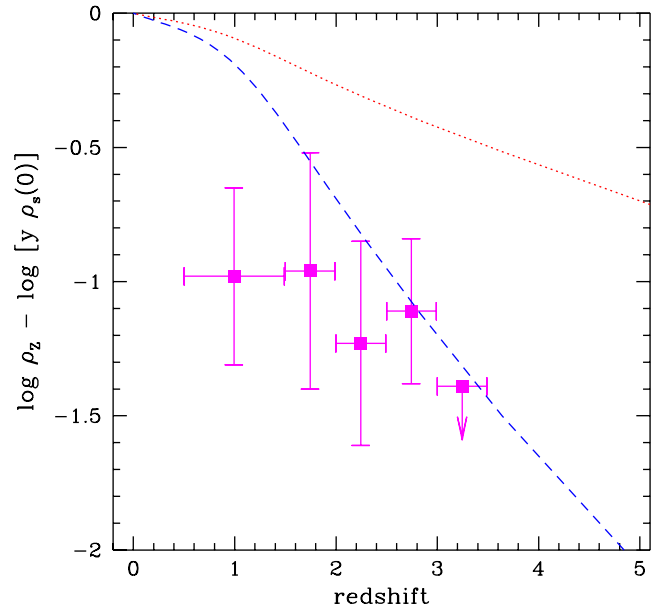


Figure 12. Total mass of heavy elements ever ejected versus redshift for the Salpeter IMF model of Figure 7 (*dashed line*) and the “monolithic collapse” model of Figure 11 (*dotted line*), normalized to $y\rho_s(0)$, the total mass density of metals at the present epoch. *Filled squares*: column density-weighted metallicities (in units of solar) as derived from observations of the damped Lyman- α systems (Pettini et al. 1997).

At early epochs, when the gas consumption into stars is still low, the metal mass density predicted from these models gives, in a closed box model, a measurement of the metallicity of the gas phase. If DLAs and star-forming field galaxies have the same level of heavy element enrichment (Pei & Fall 1995), then one would expect a rough agreement between Z_{DLA} and the model predictions at $z \gtrsim 3$. This is not true at $z \lesssim 2$, when a significant fraction of heavy elements is locked into stars. Without reading too much into this comparison (note the large error bars associated with the data points), it does appear that the monolithic collapse model tends to overpredict the cosmic metallicity at high redshifts as sampled by the DLAs.

While the detection with NICMOS of the established stellar populations surrounding the regions of star formation observed in the HDF at $z \sim 2$ should shed some light on the questions addressed in this talk, it will ultimately take the Next Generation Space Telescope to see the visible light emitted by stars at $z = 2 - 5$, and to effectively open much of the universe to a direct study of galaxy formation and the history of the conversion of neutral gas into stars.

Acknowledgments. I would like to thank G. Bruzual, S. Charlot, A. Connolly, M. Pettini, and my collaborators, L. Pozzetti and M. Dickinson, for many stimulating discussion on various topics related to this talk. Support for this work was provided by NASA through grant AR-06337.10-94A from the Space Telescope Science Institute, which is operated by the Association of Universities for Research in Astronomy, Inc., under NASA contract NAS5-26555.

References

- Baugh, C. M., Cole, S., Frenk, C. S., & Lacey, C. G. 1997, ApJ, submitted
- Bower, R. G., Lucey, J. R., & Ellis, R. S. 1992, MNRAS, 254, 589
- Bruzual, A. G., & Charlot, S. 1993, ApJ, 405, 538
- Bruzual, A. G., & Charlot, S. 1997, in preparation
- Charlot, S., Worthey, G., & Bressan, A. 1996, ApJ, 457, 625
- Cohen, J. G., Cowie, L. L., Hogg, D. W., Songaila, A., Blandford, R., Hu, E. M., & Snopbell, P. 1996, ApJ, 471, L5
- Cole, S., Aragón-Salamanca, A., Frenk, C. S., Navarro, J. F., & Zepf, S. E. 1994, MNRAS, 271, 781
- Connolly, A. J., Szalay, A. S., Dickinson, M. E., SubbaRao, M. U., & Brunner, R. J. 1997, ApJ, in press
- Cowie, L. L., Songaila, A., Hu, E. M., & Cohen, J. G. 1996, AJ, 112, 839
- Djorgovski, S., & Thompson, D. 1993, in IAU Symp. 149, The Stellar Populations in Galaxies, ed. A. Renzini & B. Barbuy (Dordrecht: Kluwer), 337
- Dickinson, M. E. 1997, private communication
- Dickinson, M. E., et al. 1997, in preparation
- Ellis, R. S., Colless, M., Broadhurst, T., Heyl, J., & Glazebrook, K. 1996, MNRAS, 280, 235

- Eggen, O. J., Lynden-Bell, D., & Sandage, A. R. 1962, *ApJ*, 136, 748
- Fall, S. M., Charlot, S., & Pei, Y. C. 1996, *ApJ*, 464, L43
- Gallego, J., Zamorano, J., Arag'ón-Salamanca, A., & Rego, M. 1995, *ApJ*, 455, L1
- Gardner, J. P., Sharples, R. M., Frenk, C. S., & Carrasco, B. E. 1997, *ApJ*, 480, L99
- Guhathakurta, P., Tyson, J. A., & Majewski, S. R. 1990, *ApJ*, 357, L9
- Guiderdoni, B., Bouchet, F. R., Puget, J.-L., Lagache, G., & Hivon, E. 1997, *Nature*, in press
- Kashlinsky, A., Mather, J. C., & Odenwald, S. 1996, *ApJ*, 473, L9
- Kauffmann, G., White, S. D. M., & Guiderdoni, B. 1993, *MNRAS*, 264, 201
- Lilly, S. J., Tresse, L., Hammer, F., Crampton, D., & Le Fèvre, O. 1995, *ApJ*, 455, 108
- Lilly, S. J., Le Fèvre, O., Hammer, F., & Crampton, D. 1996, *ApJ*, 460, L1
- Lowenthal, J. D., Koo, D. C., Guzman, R., Gallego, J., Phillips, A. C., Faber, S. M., Vogt, N. P., Illingworth, G. D., & Gronwall, C. 1997, *ApJ*, 481, 673
- Madau, P. 1995, *ApJ*, 441, 18
- Madau, P. 1997, in *Star Formation Near and Far*, eds. S. S. Holt & G. L. Mundy, (AIP: New York), p. 481
- Madau, P., Ferguson, H. C., Dickinson, M. E., Giavalisco, M., Steidel, C. C., & Fruchter, A. 1996, *MNRAS*, 283, 1388 (M96)
- Madau, P., Pozzetti, L., & Dickinson, M. E. 1997, *ApJ*, submitted
- Maeder, A. 1992, *A&A*, 264, 105
- Meurer, G. R., Heckman, T. M., Lehnert, M. D., Leitherer, C., & Lowenthal, J. 1997, *AJ*, in press
- Pagel, B. E. J. 1987, in *The Galaxy*, eds. G. Gilmore & B. Carswell (Reidel: Dordrecht), p. 341
- Pei, Y. C., & Fall, S. M. 1995, *ApJ*, 454, 69
- Pettini, M., Smith, L. J., King, D. L., & Hunstead, R. W. 1997, *ApJ*, in press
- Pozzetti, L., Madau, P., Ferguson, H. C., Zamorani, G., & Bruzual, G. A. 1997, *MNRAS*, submitted
- Puget, J.-L., Abergel, A., Bernard, J.-P., Boulanger, F., Burton, W. B., Desert, F.-X., & Hartmann, D. 1996, *A&A*, 308, L5
- Renzini, A. 1993, in *Ann. NY Acad. Sci.*, No. 688, *Proc. Texas/Pascos Symp on Relativistic Astrophysics & Particle Cosmology*, ed. C. W. Akerlof & M. A. Srednicki, 124
- Salpeter, E. E. 1955, *ApJ*, 121, 161
- Scalo, J. N. 1986, *Fundam. Cosmic Phys.*, 11, 1
- Schechter, P. L., & Dressler, A. 1987, *AJ*, 94, 56
- Soifer, B. T., & Neugebauer, G. 1991, *AJ*, 101, 354
- Steidel, C. C., Giavalisco, M., Pettini, M., Dickinson, M. E., & Adelberger, K. 1996a, *ApJ*, 462, L17

- Steidel, C. C., Giavalisco, M., Dickinson, M. E., & Adelberger, K. 1996b, AJ, 112, 352
- Steidel, C. C., & Hamilton, D. 1992, AJ, 104, 941
- Tinsley, B. M. 1980, Fundam. Cosmic Phys., 5, 287
- Tinsley, B. M., & Gunn, J. E. 1976, ApJ, 203, 52
- White, S. D. M., & Frenk, C. S. 1991, ApJ, 379, 25
- Williams, R. E., et al. 1996, AJ, 112, 1335
- Woolsey, S. E., & Weaver, T. A. 1995, ApJS, 101, 181